Turkish Journal of Earth Sciences (Turkish J. Earth Sci.), Vol. 19, 2010, pp. 367–383. Copyright ©TÜBİTAK
doi:10.3906/yer-0812-7 First published online 20 July 2009

The Impact of Tsunamis on the Island of Majorca induced by North Algerian Seismic Sources

JOSÉ A. ÁLVAREZ-GÓMEZ[1], MAITANE OLABARRIETA[2], MAURICIO GONZÁLEZ[2], LUÍS OTERO[2,3], EMILIO CARREÑO[4] & JOSÉ M. MARTÍNEZ-SOLARES[4]

[1] TRANSFER Project, Centro Nacional de Información Geográfica. C/General Ibáñez Ibero, nº3, 28003 Madrid, Spain (E-mail: jaagomez@fomento.es)

[2] Ocean & Coastal Research Group, Instituto de Hidráulica Ambiental "IH Cantabria", Universidad de Cantabria, E.T.S. Ingenieros de Caminos, C. y P., Av. de los Castros, s/n. 39005 Santander, Spain

[3] Dirección General Marítima. Ministerio de Defensa Nacional, Armada Nacional, Av. El Dorado CAN, Bogota, Colombia

[4] Instituto Geográfico Nacional. C/ General Ibáñez Ibero, nº3, 28003 Madrid, Spain

Received 04 December 2008; revised typescript receipt 23 August 2009; accepted 03 July 2009

Abstract: The north of Algeria is the main earthquake-related tsunami generation zone that threatens the Balearic Islands. In this work we review the major seismic series of the area –the 1980 El Asnam and the 2003 Boumerdes-Zemmouri earthquakes– in order to obtain a probable worst characteristic earthquake rupture. We estimate rupture dimensions of 55 km × 16 km, reaching the fault plane a depth of 13 km. The dip and rake have been taken as constants, with values of 50° and 90° respectively, while the strike is adjusted to the local tectonic structure. With these characteristics a magnitude M_W= 7.3 earthquake is obtained for an average slip of 4 metres; these values being reasonable for the seismotectonics of the area. Nine sources along the northern coast of Algeria have been proposed, some of them have been mapped offshore and others that are less known are probable continuations of onshore structures. Based on numerical simulations the tsunami impacts of the nine potential events on Majorca have been studied. Catastrophic tsunamis cannot be triggered from these sources in the Balearic Islands. However, wave elevations up to 2 m can generate flooding in low areas and wave amplifications in bays and harbours that can be damaging, as witnessed in historical events.

Key Words: Mediterranean Sea, Balearic Islands, Majorca, Algeria, tsunamis, seismotectonics

Kuzey Cezayir Sismik Kaynaklarından Uyarılmış Tsunami Dalgalarının Majorca Adasındaki Etkileri

Özet: Kuzey Cezayir Balearic adalarını tehdit eden deprem kaynaklı tsunami dalgalarının kaynaklandığı ana bölgeyi oluşturmaktadır. Bu çalışmada olası en kötü deprem yırtığını tesbit etmek amacına yönelik olarak 1980 El Asnam ve 2003 Boumerdes-Zemmouri depremleri gibi önemli deprem serileri incelendi. Yaklaşık 13 km derinlikte bulunan fay düzlemine kadar ulaşan deprem yırtığının boyutları 55 km × 16 km olarak tahmin edildi. Doğrultu lokal tektonik yapıya uyarlanırken, eğim ve yan yatma açıları sabitler olarak kabul edildi ve değerleri sırasıyla 50° ve 90° olarak değerlendirildi. Bu karakteristik özellikler dikkate alınarak 4 metrelik ortalama bir kayma miktarı için deprem büyüklüğü M_W= 7.3 olarak hesaplandı; bu değerler bölgenin sismotektonik özellikleriyle uyumludur. Ceyazir'in kuzey kıyılarında dokuz farklı kaynak önerilmiştir; kaynakların bazıları kıyıdan uzak açık denizde haritalanırken, daha az bilinen diğer kaynaklar olasılıkla kıyıya yakın yapıların devamı niteliğindedir. Sayısal simülasyon çalışmaları ile potansiyel dokuz depremin yaratacağı olası tsunami dalgalarının Majorca adası üzerindeki etkileri çalışıldı. Bu kaynaklardan Balearic Adalarında felaket getirecek tsunami dalgalarının tetiklenemeceği görüldü. Ancak, tarihi depremlerde olduğu gibi dalga yükselikleri 2 metreyi bulacak tsunamiler alçak alanlarda, dalga büyümesi ise koy ve limanlarda sele neden olabilir.

Anahtar Sözcükler: Akdeniz, Balearic Adaları, Majorca, Cezayir, tsunami, sismotektonik

Introduction

During the past few centuries, the Balearic Islands have been affected by the occurrence of several tsunamis caused along the northern coast of Africa, mainly on the Algerian coast (IGN 2008). At least four events have been reported: 1756, 1856, 1980 and 2003. There is little information about the first event and the reliability of the source is low (IGN 2008). For the 1856 tsunami the information on damage refers mainly to the Algerian coast, in the area of Jijel and Béjaïa (Bougie). In 1980, the mareographs of the Balearic Islands reported variations in the wave amplitude due to the magnitude 7.3 El Asnam earthquake, with an epicentre 30–40 km inland from the coast (Ouyed *et al.* 1981). In 2003 the main damage was to the harbours, where hundreds of boats sank or were damaged along the southern coasts of Majorca and Minorca, and wave amplitudes higher than 1 m were reported. This magnitude M_W= 6.9 event took place off the coast of Boumerdes-Zemmouri, in Algeria, south of Majorca (IGN 2003; Bounif *et al.* 2004; Delouis *et al.* 2004).

There is a lack of knowledge about the tsunami hazard that the tectonic structures of the northern Algerian coast poses for the Balearic Islands and the Mediterranean coast of the Iberian Peninsula. In previous years, and following the 2003 Boumerdes-Zemmouri earthquake and tsunami, several works were produced studying the tsunami impact of this very source, although they omitted discussion of remaining potential sources (Hébert & Alasset 2003; Wang & Liu 2005; Alasset *et al.* 2006). In this context we study the tsunami hazard related to the active tectonic structures that border the northern African coast of Algeria. We have reviewed the data concerning the 1980 El Asnam and 2003 Boumerdes-Zemmouri earthquakes in order to obtain credible fault and earthquake dimensions for modelling purposes. We have distributed our modelling fault along the northern coast of Algeria, adapting it to the local structure, and have generated tsunami propagation models to study the potential hazard of each source.

The main objectives of this work are: (1) to obtain a set of possible tsunamigenic sources along the northern coast of Algeria; (2) to assess the worst potential seismic sources for the tsunami hazard in the Balearic Islands; and (3) to evaluate the tsunami impact of the different tsunami sources in Majorca using numerical simulations.

Seismotectonics and Seismic Source Analysis

The Northern African coast bounds the Rif-Tell-Atlas mountain range (Figure 1). An orogenic system developed from the Palaeocene–Eocene to the present, in the context of the Alpine orogeny, mostly configures the present geography of the Mediterranean shores. The active deformation of the area is caused by the NNW motion of the African plate towards the Eurasian plate, taking the latter as fixed. The rate of motion is 4–6 mm/yr (DeMets 1990; McClusky *et al.* 2003; Serpelloni *et al.* 2007), and started 9 million years ago, in the late Miocene (Galindo-Zaldívar *et al.* 1993). This motion is accommodated here by a system of thrust and folds striking NE–SW, with a double vergence, towards both the southeast and northwest. These structures are interpreted in the context of a transpressive system (Morel & Meghraoui 1996). This area is absorbing around 2–4 mm/yr (40–60%) of the total convergence between the plates (Meghraoui & Doumaz 1996; Morel & Meghraoui 1996; Serpelloni *et al.* 2007). The mentioned tectonic structures, frequently known as seismogenic inland (Bezzeghoud *et al.* 1995; Yelles-Chaouche *et al.* 2003), have their continuation offshore and are the most probable sources of tsunamis in the area (Alasset *et al.* 2006).

In order to establish a characteristic source for the area, following the approximation of Lorito *et al.* (2008), we have reviewed the proposed sources for the major earthquakes: M_W 7.1, 1980 El Asnam earthquake, and M_W 6.9, 2003 Boumerdes-Zemmouri earthquake. As the active offshore structures are continuations of the onshore tectonic belts (Bounif *et al.* 2004; Meghraoui *et al.* 2004; Déverchère *et al.* 2005) we can assume similar rupture processes in both environments, and then we can consider these two historic events as representative of the regional active deformation.

Field work and observations following the 1980 El Asnam earthquake (Ambraseys 1981; King & Vita-Finzi 1981; Ouyed *et al.* 1981; Ruegg *et al.* 1982; Philip & Meghraoui 1983), showed that the average

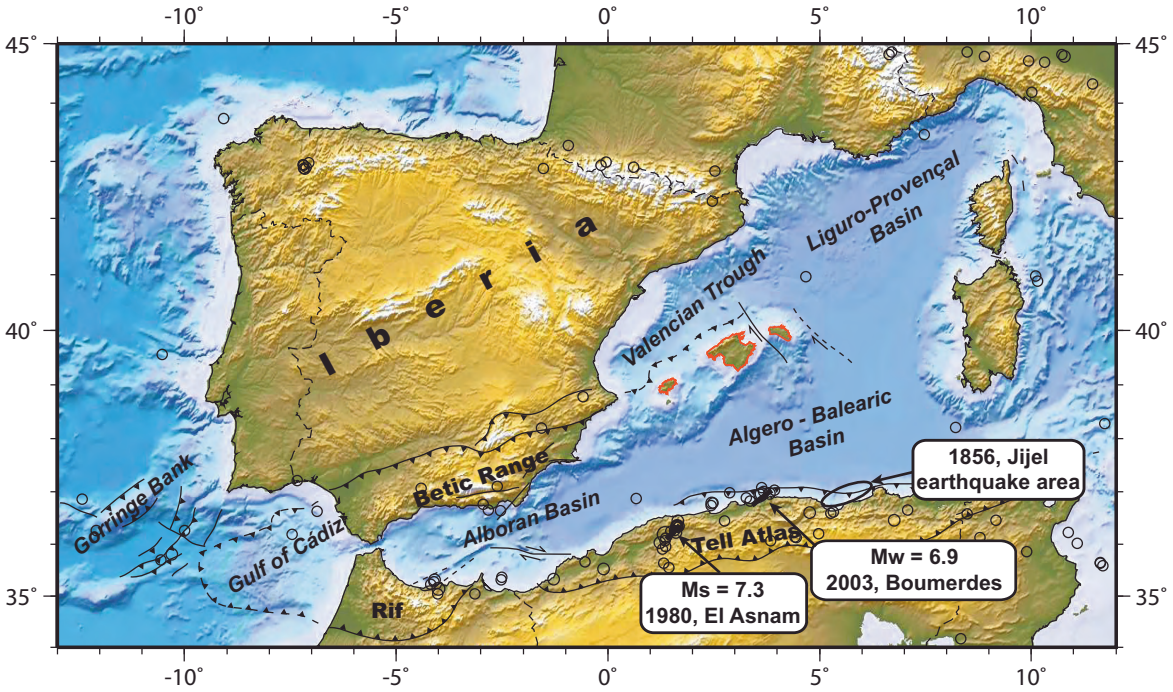

Figure 1. Tectonic setting of the study area showing the main structural boundaries. Lines with triangles show the limits between the Betic-Rif-Tell orogen and the foreland; except in the Gorringe Bank area, where they show the main compressive structures. Thick lines are the limits between the internal and external zones of the orogen. Thin lines are relevant strike-slip faults. Circles show shallow seismicity with magnitudes $M_W > 5$ from the NEIC catalogue. Dark shaded areas are the Balearic Islands.

vertical displacement was 2–3 m, with the displacement of the fault being almost purely thrust, although with minor strike-slip and normal cracks and faulting at the surface (Philip & Meghraoui 1983), with 1.8–2.5 m of shortening and maximum vertical displacements of around 6 m. The reported moments of this event varies according to the method used to obtain it (Ruegg *et al.* 1982), giving moment magnitudes, M_W, that range from 6.83 to 7.20. The surface rupture had a NE–SW trend and a length of 35–40 km, while the subsurface extension can be estimated as 55 km (Ruegg *et al.* 1982). The selected fault plane from the focal mechanism dips 50° towards the NW and strikes in the same direction as the surface rupture (Deschamps *et al.* 1982). The analysis of the aftershocks led to the conclusion that the fault plane adopts listric geometry at the depth of 9–10 km (Yielding *et al.* 1989). Some of the proposed source models parameters are summarised in Table 1.

For the 2003 Boumerdes-Zemmouri earthquake, several fault plane solutions and source parameters have been proposed (Table 2). Alasset *et al.* (2006) reviewed some of the sources and concluded that the Meghraoui *et al.* (2004) and Delouis *et al.* (2004) sources are the most feasible. These two sources show a rupture of 55 km × 16 km, with the strike varying from N55°E to N70°E and a dip of 45–50°; in both cases the rake is almost pure thrust (90–95°). The analysis and relocation of the 2003 seismic series show the events following a planar distribution striking N55–60°E and dipping 45–55°, reaching a depth of 16 km (Bounif *et al.* 2004). The observed structure is the offshore continuation of the Blida thrust fault system (Bounif *et al.* 2004; Meghraoui *et al.* 2004). The offshore area of the Algerian coast from Algiers to Dellys, which includes the Boumerdes-Zemmouri zone, was mapped recently by Déverchère *et al.* (2005). They mapped a system of thrust and folds with NW vergence. In this system,

Table 1. Previously proposed source parameters for the 1980 El Asnam earthquake.

M_W	Depth (km)	Strike (°)	Dip (°)	Rake (°)	Fault Length (km)	Fault Width (km)	Reference
7.20	8*	230	52	90	40	19	Ouyed *et al.* 1981
7.17	10	230	54	85	32	18.5	Deschamps *et al.* 1982**
7.16	7*	232	60	70	36	16	Ruegg *et al.* 1982**
7.34	6*	222	45	75	63	19	Nábělek 1985**
7.09	5*	227	60	90	21	12	Bezzeghoud *et al.* 1995**

* Mean depth of the fault plane.
** Source parameters are averaged values and total dimensions from the original segmented sources.

Table 2. Previously proposed source parameters for the 2003 Boumerdes-Zemmouri earthquake.

M_W	Depth (km)	Strike (°)	Dip (°)	Rake (°)	Fault Length (km)	Fault Width (km)	Reference
6.9	10	54	47	86	65	17	Yagi 2003
6.8	8	54	50	90	54	15	Meghraoui *et al.* 2004
6.9	6.5	70	45	95	55	13	Delouis *et al.* 2004
6.8	9	55	42	84	32	14	Yelles *et al.* 2004
6.7	8	64	50	111	50	16	Bezzeghoud *et al.* 2006**
7.1	16	54	47	90	64	32	Semmane *et al.* 2005

* Mean depth of the fault plane. ** As cited in Alasset *et al.* (2006).

the presence of piggy-back basins allowed them to estimate an uplift rate of 0.2 mm/yr on one of the main thrusts.

Synthetic Source Model

From the reviewed seismic sources we can establish a characteristic credible tsunamigenic earthquake for the area. A common feature is the orientation, approximately NE–SW, with a rake of almost pure thrust faulting, which is coherent with the NW–SE-directed active stress field (Serpelloni *et al.* 2007). The dip direction in the El Asnam earthquake is towards the northwest, although the main part of the thrust system running offshore towards Tunisia, and responsible for the 2003 Boumerdes-Zemmouri earthquake, has the opposite vergence, with these faults dipping southwards (Yelles *et al.* 2007). Fault planes dipping southeast and situated offshore are capable of generating worse tsunamis for the Balearic Islands than those dipping northwest, which are mainly present onshore.

The dimensions of the plane are based on field observations of the surface ruptures and on the characteristics of the seismic series. A fault length of 55 km has been taken as reasonable, and a maximum depth of 13 km, which gives a width of approximately 16 km. The maximum depth is taken as a reasonable value for the seismogenic layer in the area (Mickus & Jallouli 1999) and is coherent with the observations that show how the seismic deformation has mainly been concentrated in the upper 10–12 km of the crust in previous seismic series (Chiarabba *et al.* 1997; Bounif *et al.* 2004). From these dimensions an earthquake magnitude M_W 7.3 is obtained with a mean slip over the fault of 4 m (following the seismic moment definition with a crustal shear modulus of 0.3 x 10^{10} Pa). This magnitude is likely to be the probable maximum

earthquakesize for the area (Aoudia *et al.* 2000; Peláez Montilla *et al.* 2003). The rake and dip of the fault are constant in the sources, being pure reverse faulting (90°) with a dip of 50°. The direction varies according to the local trends and, in addition to the NE–SW structures, we have also modelled some offshore E–W structures dipping south (Déverchère *et al.* 2005; Domzig *et al.* 2006). In Figure 2 some of the main active structures are shown, compiled from Meghraoui & Doumaz (1996), Aoudia *et al.* (2000), Harbi *et al.* (2003), Déverchère *et al.* (2005), Alasset *et al.* (2006), Domzig *et al.* (2006) and Yelles *et al.* (2007).

We propose nine different sources along the northern coast of Algeria (Table 3, Figure 2). Four of them trend approximately E–W (S-1, S-2, S-3 and S-5); these faults have been partially mapped by Domzig *et al.* (2006). Source S-4 corresponds to the fault responsible for the 2003 Boumerdes-Zemmouri earthquake (Table 2), although presenting a higher seismic magnitude for our numerical model. Sources S-6, S-7, S-8 and S-9 are considered to be continuations of the active fold and thrust belt structures inland. Movement on one of the faults in the Béjaïa-Jijel area (S-6, S-7 and S-8) could well be the cause of the 1856 Jijel earthquake and tsunami.

Tsunami Hazard in Majorca

Numerical Model Description

COMCOT (Cornell Multi-grid Coupled Tsunami Model) is the finite difference scheme numerical model used in the present study. The model has been used to investigate several historical tsunami events, such as the 1960 Chilean tsunami (Liu *et al.* 1994), the 1992 Flores Islands (Indonesia) tsunami (Liu *et al.* 1995), the 2004 Indian Ocean tsunami (Wang & Liu 2005) and the Algerian 2003 tsunami (Wang & Liu 2005). The model has also been validated using the benchmark cases proposed in the working frame of the European Tsunami Project TRANSFER.

It solves both non linear and linear shallow water equations, adopting a modified leap-frog scheme. Its nesting capabilities make it possible to simulate tsunami generation and its propagation from the source zone to a given coastal area, considering the possible inundation of coastal zones. A two-way nesting method is applied for the nested grid system. The finer inner grid adopts a smaller grid size and time step compared to its adjacent outer (larger) grid. In the outer grid, at the beginning of a time step, the volume flux is interpolated into its inner (finer) grid. At the end of this time step, the calculated water surface elevations at the inner finer grids are averaged to update the free surface elevations of the larger grids, which are used to compute the volume fluxes at the next time step in the coarse grids (Wang & Liu 2005). By this method, the model is able to capture near-shore features of tsunami propagation with higher grid and time resolution while maintaining computational efficiency (Wang & Liu 2005).

In the Mediterranean region, earthquake-generated tsunamis are expected to produce wave

Table 3. Proposed potential seismic tsunamigenic sources.

	Fault tips(Lat – Lon)				km	km	km	km	º	º	º		m
Source	x1	y1	x2	y2	Top	Bottom	Length	Width	Dip	Strike	Rake	M_W	Slip
S-1	1.262	36.700	1.881	36.738	0.5	13	55	16	50	0.86	90	7.3	4
S-2	1.869	36.842	2.480	36.919	–	–	–	–	–	0.81	–	–	–
S-3	2.583	36.961	3.204	36.962	–	–	–	–	–	0.90	–	–	–
S-4	3.449	36.809	3.964	37.084	–	–	–	–	–	0.56	–	–	–
S-5	4.082	37.085	4.703	37.071	–	–	–	–	–	0.92	–	–	–
S-6	4.576	36.905	5.119	37.146	–	–	–	–	–	0.61	–	–	–
S-7	5.400	36.713	5.916	36.988	–	–	–	–	–	0.56	–	–	–
S-8	5.916	36.988	6.472	37.207	–	–	–	–	–	0.64	–	–	–
S-9	6.637	36.981	7.180	37.221	–	–	–	–	–	0.61	–	–	–

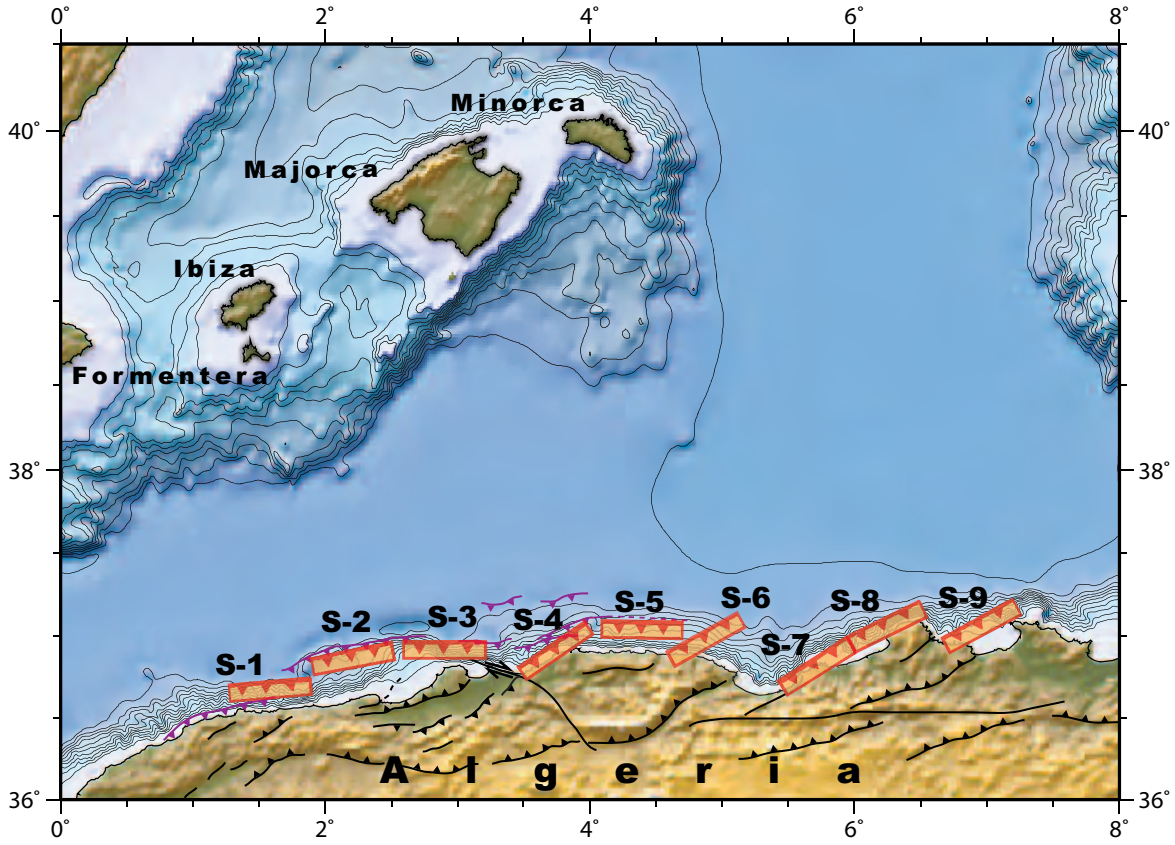

Figure 2. Map of proposed seismic tsunamigenic sources (S-1…S-9) and its situation with respect to the Balearic Islands. The structures shown have been compiled from the works of Meghraoui & Doumaz (1996), Aoudia *et al.* (2000), Harbi *et al.* (2003), Déverchère *et al.* (2005), Domzig *et al.* (2006), Alasset *et al.* (2006) and Yelles *et al.* (2007). Bathymetry and topography is from the Global GEBCO Grid, isobath interval is 250 m.

lengths between 150 and 5 km (Wang & Liu 2005), depending on the water depth. In the deepest areas, with water depths around 3 km, the tsunami wave length is about 100 km while in shallow areas this value decreases to 5 km approximately. In these circumstances, wave dynamics can be considered mainly horizontal, with negligible vertical accelerations and thus the pressure field can be assumed to be hydrostatic. The propagation of this kind of wave can be correctly simulated using the shallow water wave equations. In a Cartesian coordinate system these equations can be expressed as:

Mass Conservation Equation

$$\frac{\partial \zeta}{\partial t} + \frac{\partial P}{\partial x} + \frac{\partial Q}{\partial x} = 0 \qquad (1)$$

Momentum Conservation Equations:

$$\frac{\partial P}{\partial t} + \frac{\partial P^2}{\partial x} + \frac{\partial PQ}{\partial y} + gH\frac{\partial \zeta}{\partial y} + \tau_x H - fQ = 0 \qquad (2)$$

$$\frac{\partial P}{\partial t} + \frac{\partial PQ}{\partial x} + \frac{\partial Q^2}{\partial y} + gH\frac{\partial \zeta}{\partial y} + \tau_y H - fP = 0 \qquad (3)$$

where ζ is the free surface elevation above mean sea level; *(x,y)* represent the longitude and latitude of the earth; (τ_x, τ_y) are the bottom shear stress in *x* axis (easting) and *y* axis (northing); *P* and *Q* stand for the

volume fluxes ($P=Hu$ and $Q=Hv$ with u and v being the depth-averaged velocities in the longitude and latitude direction); H is the total water depth $(=h+\zeta)$ with h being the still water depth; and f represents the Coriolis parameter.

The bottom shear stress in the simulations was modelled using the Manning's formula given by the following expression:

$$\tau_x = \frac{gn^2}{H^{10/3}} P\,(P^2 + Q^2)^{1/2}$$

$$\tau_y = \frac{gn^2}{H^{10/3}} Q\,(P^2 + Q^2)^{1/2}$$

where n is the Manning roughness coefficient. The Manning coefficient in the simulations was set to 0.02.

Model Set-up

The simulation domain, which covers a large part of the western Mediterranean region, has been computed using two nested grids (see Figure 3). The coarsest grid is 864 km long and is composed of 1001*1001 nodes in x and y axis respectively (grid size of 864m). The lower left corner of this grid is located at (0°W, 36°N). The finest grid has a dimension of 342*252 nodes, with a grid size of 432 m.

The bathymetry used in the following simulations is a composite of the bathymetric data set GEBCO, nautical charts available for the Balearic Island region and local bathymetries in the bay of Majorca from the Spanish Harbour Authorities. In Figure 3 the bathymetry corresponding to each grid considered is depicted. It is noteworthy that in most of the considered domain the water depth exceeds 1000 m. However, closer to the coast of the Iberian

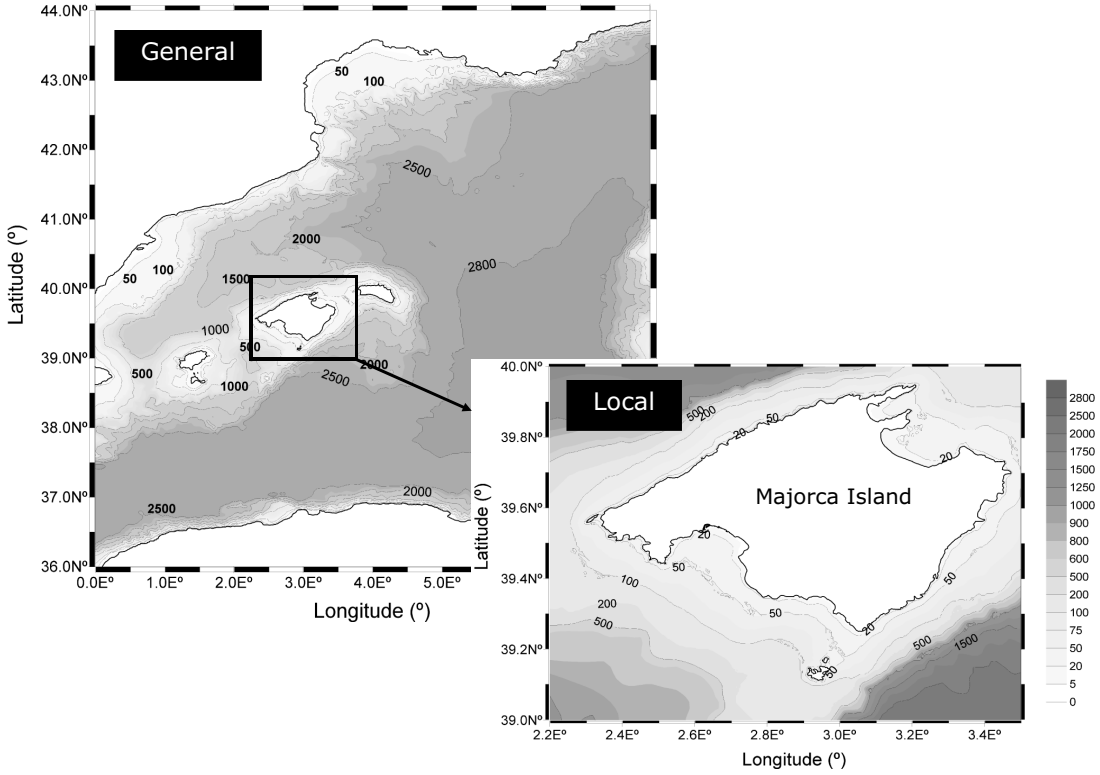

Figure 3. Western Mediterranean bathymetry corresponding to each computational grid (general and local scales).

Peninsula as well as around the Balearic Islands, the existence of continental shelf reduces the mean water depth approximately to 100 m. Around the Balearic Islands the mean width of the continental shelf is about 15 km. The existence of this continental shelf is of great importance as will be described later on.

For all the numerical simulations a radiation boundary condition has been considered in all the boundaries falling within the marine area. However, in all those boundaries separating wet and dry domains, a vertical wall condition has been adopted.

Nine different scenarios, each representing the worst fault scenario that could take place in the Algerian region (S1-S9), have been run applying the aforementioned numerical model. The free surface elevation due to each earthquake has been calculated using the equations of Okada (1985), in which an elastic dislocation is assumed. For each fault plane model a 2-hour physical duration tsunami propagation has been simulated, which took about 1.5 hours CPU time on a PENTIUM 4 desktop computer with 1 GB RAM.

Wave Elevations and Tsunami Travel Time Around Majorca

As a result of each run, the time variation of the free surface is obtained in all the computational nodes. For example, in Figure 4 the time series of the spatial variation of the free surface elevation along the general grid domain is shown. This snapshot represents the initial water displacement generated by the earthquake corresponding to the S-3 fault scenario. In the same figure the time variations of the free surface elevation at two different points are presented. The continuous line represents the point located in the source region, while the dashed line represents the point located further north. As can be appreciated at the source region, a first wave peak with a water elevation of approximately 1.5 m is observed. This is followed by the wave trough and

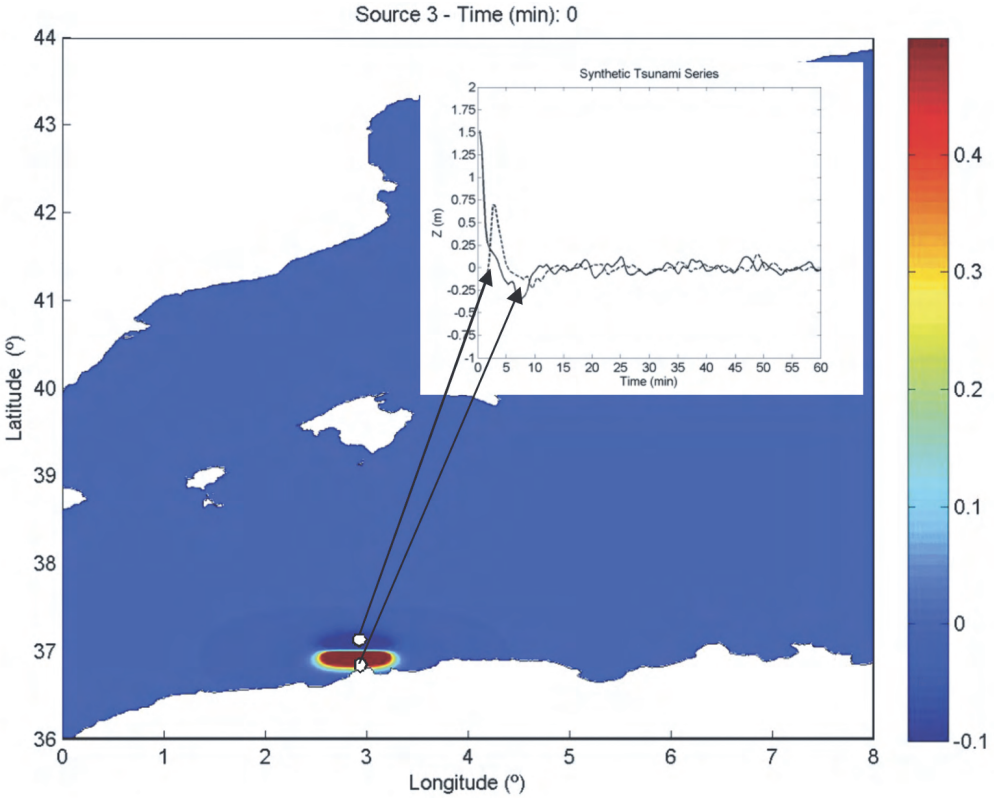

Figure 4. Initial surface deformation corresponding to the S-3 scenario and time evolution of sea level in the source zone (continuous line) and in a point located further north (dashed line).

several consecutive waves, generated by the reflections of the initial tsunami wave along the Algerian coast. These consecutive waves have less energy than the initial wave and have periods that differ from that of the initial wave, indicating non linear transferences between different frequency components.

As time goes by (see Figure 5) the tsunami propagates north. Due to the bathymetry changes, and especially due to the existence of a pronounced continental shelf around the Balearic Islands, the tsunami wave suffers an important refraction, changing the wave front directions and making them perpendicular to the continental shelf. In this specific scenario (S-3) the southeast coast of Majorca receives the greatest impact of the tsunami wave. It is noteworthy that the generation of edge waves around the Balearic Islands, represents waves trapped at the continental shelf due to the refraction effect.

In order to analyse the differential impact of each fault scenario on Majorca, and thus identify the most dangerous fault scenarios, the distribution of tsunami energy around Majorca has been computed. In Figure 6 the maximum tsunami wave elevation in the finer computational grid for each scenario considered is depicted. The first conclusion from these results is that the eastern coast of Majorca is the area most exposed to tsunami impact. However, depending on the scenario, the specific area where the severity of the tsunami impact becomes higher and its severity change may vary. Depending on the tsunami impact along the coast of Majorca, the nine fault scenarios can be divided into three different groups, described below:

The **first group**, composed of scenarios S-1 and S-2, generates a bigger impact on the southern coast of Majorca, especially in its southwest corner. The maximum wave elevation field is similar in both cases, with the difference that the second tsunami

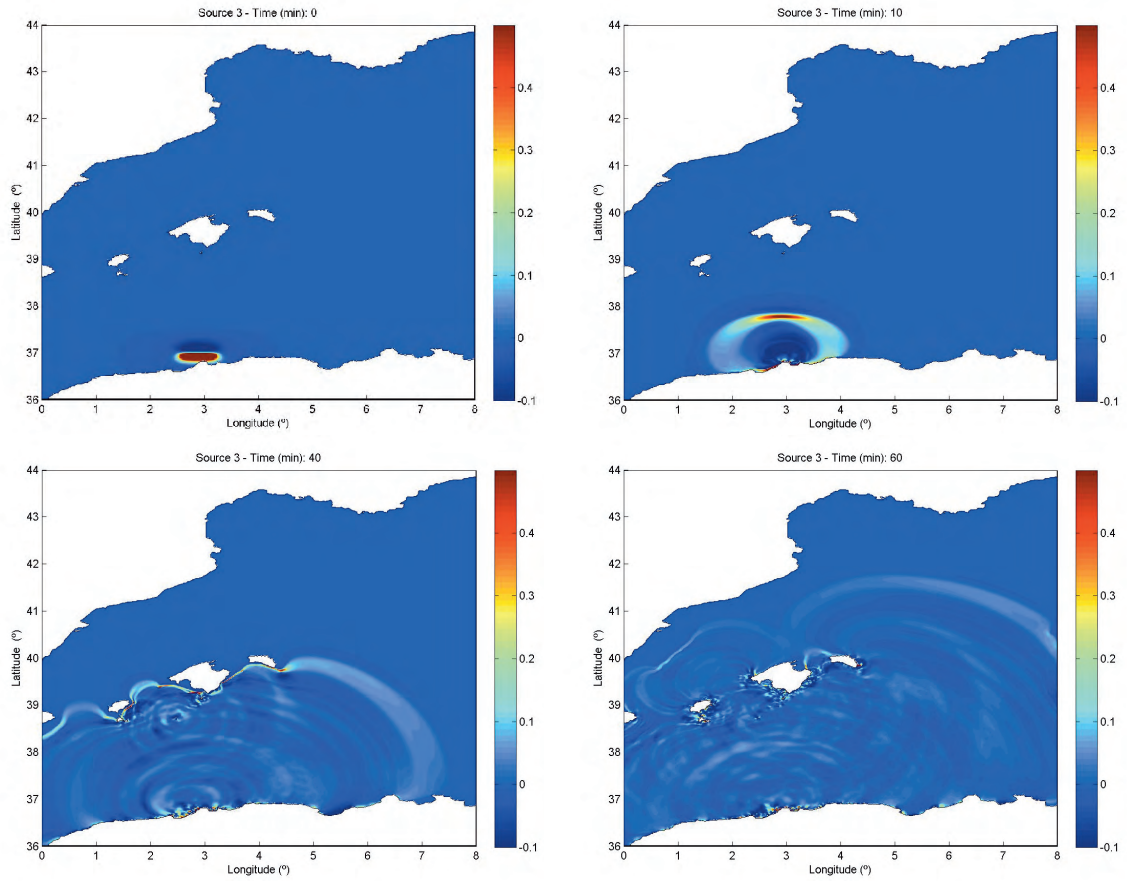

Figure 5. Snapshots of the S-3 tsunami propagation from the Algerian coast to the Balearic Islands.

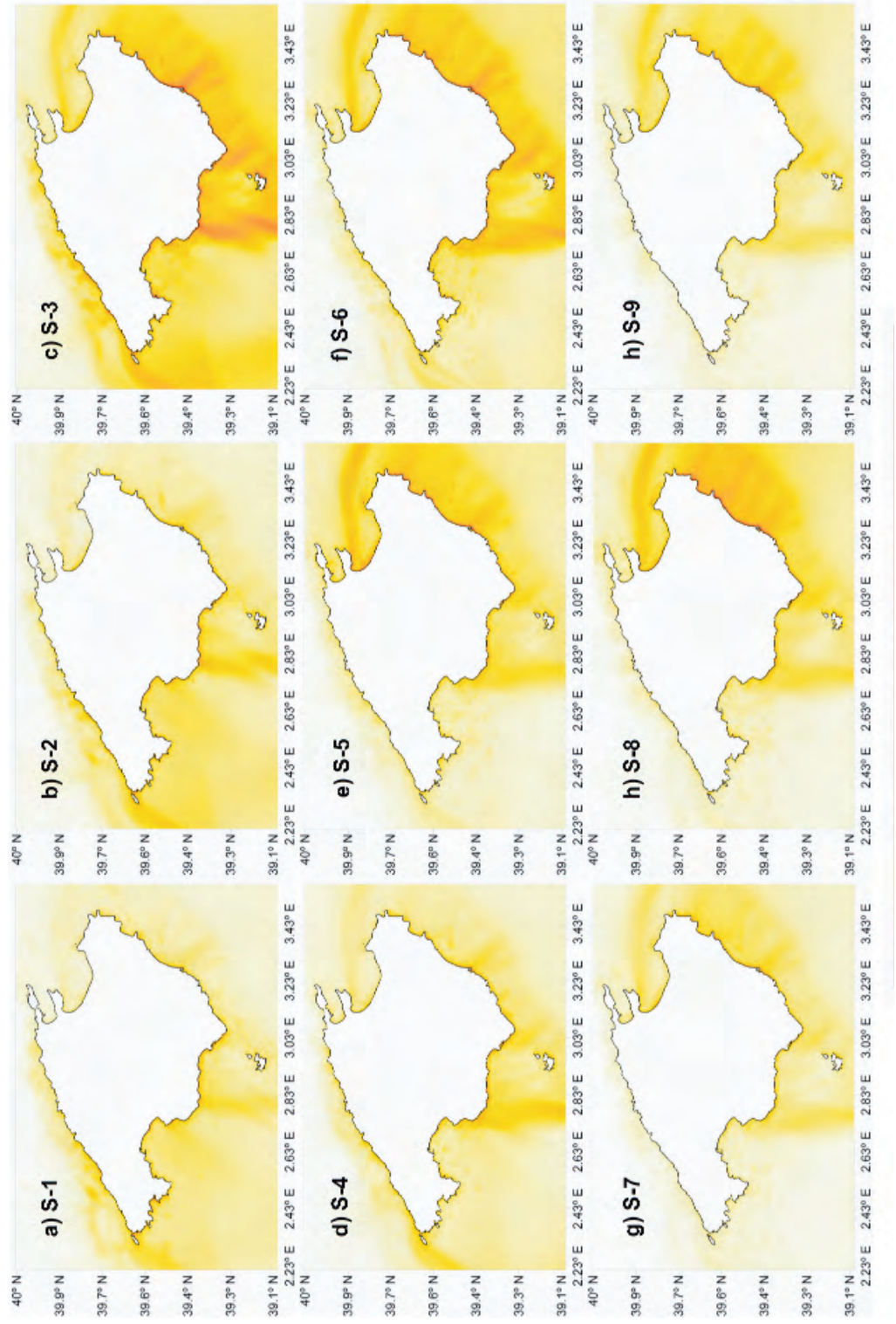

Figure 6. Maximum tsunami wave elevations in Majorca for the nine earthquake scenarios considered: (**a**) fault scenario S-1; (**b**) fault scenario S-2; (**c**) fault scenario S-3; (**d**) fault scenario S-4; (**e**) fault scenario S-5; (**f**) fault scenario S-6; (**g**) fault scenario S-7; (**h**) fault scenario S-8; and (**i**) fault scenario S-9.

scenario creates a slightly more energetic tsunami. In this case the maximum wave elevation does not exceed 0.5 m, except in very specific locations in the southwest corner, where maximum wave heights of 1.1 m are achieved. These fault scenarios are located in the western part of the Algerian coast, both having similar strike angles.

The **second group** includes the S-3, S-4 and S-6 fault scenarios. In all these cases, the biggest impact is concentrated along the eastern coast of Majorca, in the south-east corner and also in the northeast corner. Of these fault scenarios, the S-3 and S-6 scenarios create the biggest impact on Majorca, with a maximum wave elevation reaching 2.0 m in the northeast corner. It is remarkable that this group represents the one that creates the most energetic edge waves along the east coast of Majorca. All the fault scenarios within this group are located in the central part of the Algerian coast, but they have very different strike angles. While the S-3 fault, in the west, has a strike angle of 90°, the S-4 and S-6 scenarios, (further east) have strikes of 56 and 61°.

The **third group** includes those faults located in eastern Algeria (S-7, S-8, S-9) and also S-5. The biggest impact zone generated by this group is in the north-east corner of Majorca. The continental shelf that links Majorca and Minorca, characterized by a water depth of about 60 m, generates an important refraction in the incident tsunami and finally concentrates its energy in the northern part of the island. This is the reason why a direct impact of tsunamis is shown in this part of the coast. The fault S-7 is partially located inland and thus, creates a less energetic tsunami, but the S-5 and S-8 scenarios are those creating the greatest tsunami wave elevations in the north. These are characterized by different strike angles and also by different locations: S-5 is located in the central part of the Algerian coast while the other is located in the eastern part. In spite of that, both fault scenarios generate a similar impact on Majorca.

Similar conclusions can be drawn if the maximum achieved wave elevation in different locations along the Majorca coast is represented for the different potential fault scenarios. All the considered points are located in a water depth of 10 m (Figure 7). In Figure 8 the maximum wave elevations for the 9 modelled sources at each considered point are shown as histograms: the exact values are given in Table 4.

Points 1 and 2 (Figures 7 & 8) are located on the north coast of Majorca, where, especially in Pollensa Bay (Point 2), the S-5 scenario is the most dangerous, creating wave elevations up to 1.8 m. In the northern part the severity of tsunami impact is lower. Points 3 to 6 are located along the eastern coast of Majorca: Point 4 receives the greatest tsunami impact. The maximum wave elevation for the S-6 fault scenario (at this point) exceeds 2 m. In the northern part of the east coast the S-6 and S-8 scenarios have the largest impact, while in the southern part of this coast the tsunami impact becomes less severe, but not negligible, with the second group of scenarios (S-3, S-4 and S-6) being the strongest.

In the southern coast of Majorca (points 7 to 10) 1 m wave elevations can be achieved, especially along the western coast, where the most energetic tsunamis are obtained from the first three fault scenarios (S-1, S-2 and S-3).

Finally, on the west coast of Majorca (points 11 and 12), the effect of the possible tsunamis is smaller than anywhere along the island. Even so, the S-3 tsunami scenario generates wave elevations reaching 0.75 m.

The tsunami travel time in the twelve points around Majorca has been computed by each potential fault scenario (S-1 to S-9), and summarized in Table 5. Note that the minimum tsunami travel time is 31 minutes for Point (P6), and the maximum travel time (to Point P2) is 80 minutes.

It is noteworthy that the Boumerdes-Zemmouri earthquake of May 21 2003, that caused severe economic damage, especially in Palma de Majorca harbour, was generated by the S-4 tsunami source. It was less energetic than the worst case S-4 scenario in which the earthquake magnitude is considered 7.3 M_W, as the 2003 Boumerdes-Zemmouri tsunami was generated by an earthquake of magnitude 6.9 M_W (Meghraoui *et al.* 2004). Maximum sea levels rises around the Balearic Islands (Ibiza and Majorca) for this real event are reported to have been as high as 0.7 m (Alasset *et al.* 2006). It can be seen that the maximum wave elevation achieved around Majorca for the S-4 scenario does not exceed 1 m. Even this

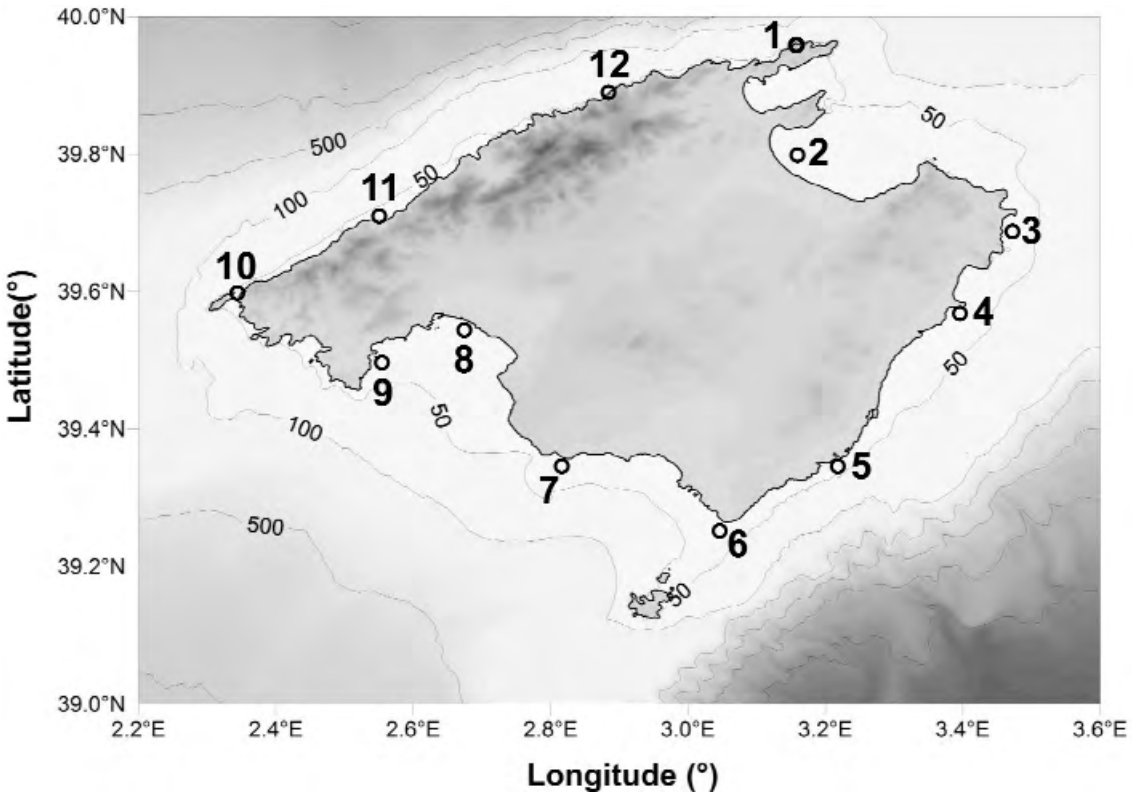

Figure 7. Location of the selected points on the Majorca coast with a depth of 10 m.

Table 4. Maximum free surface displacement in different points located around Majorca for tsunamis generated by each potential source (in meters).

points	S-1 m.	S-2 m.	S-3 m.	S-4 m.	S-5 m.	S-6 m.	S-7 m.	S-8 m.	S-9 m.
P1	0.25	0.26	0.75	0.40	0.73	0.62	0.23	0.35	0.26
P2	0.27	0.27	0.63	0.44	1.62	1.10	0.58	1.20	0.75
P3	0.50	0.37	0.76	0.52	0.88	0.76	0.57	0.87	0.68
P4	0.71	0.73	1.37	0.86	1.50	2.05	0.82	1.75	0.88
P5	0.50	0.67	1.72	0.73	1.02	1.37	0.71	1.04	0.83
P6	0.45	0.37	0.76	0.45	0.50	0.74	0.37	0.50	0.45
P7	0.50	0.60	1.10	0.73	0.65	0.78	0.45	0.65	0.45
P8	0.30	0.61	0.50	0.26	0.25	0.58	0.25	0.28	0.22
P9	1.00	0.75	1.18	0.75	0.60	0.75	0.38	0.74	0.39
P10	1.17	1.00	1.10	0.60	0.50	0.60	0.25	0.26	0.25
P11	0.40	0.38	0.75	0.40	0.25	0.26	0.10	0.23	0.12
P12	0.25	0.22	0.26	0.12	0.25	0.20	0.10	0.12	0.10

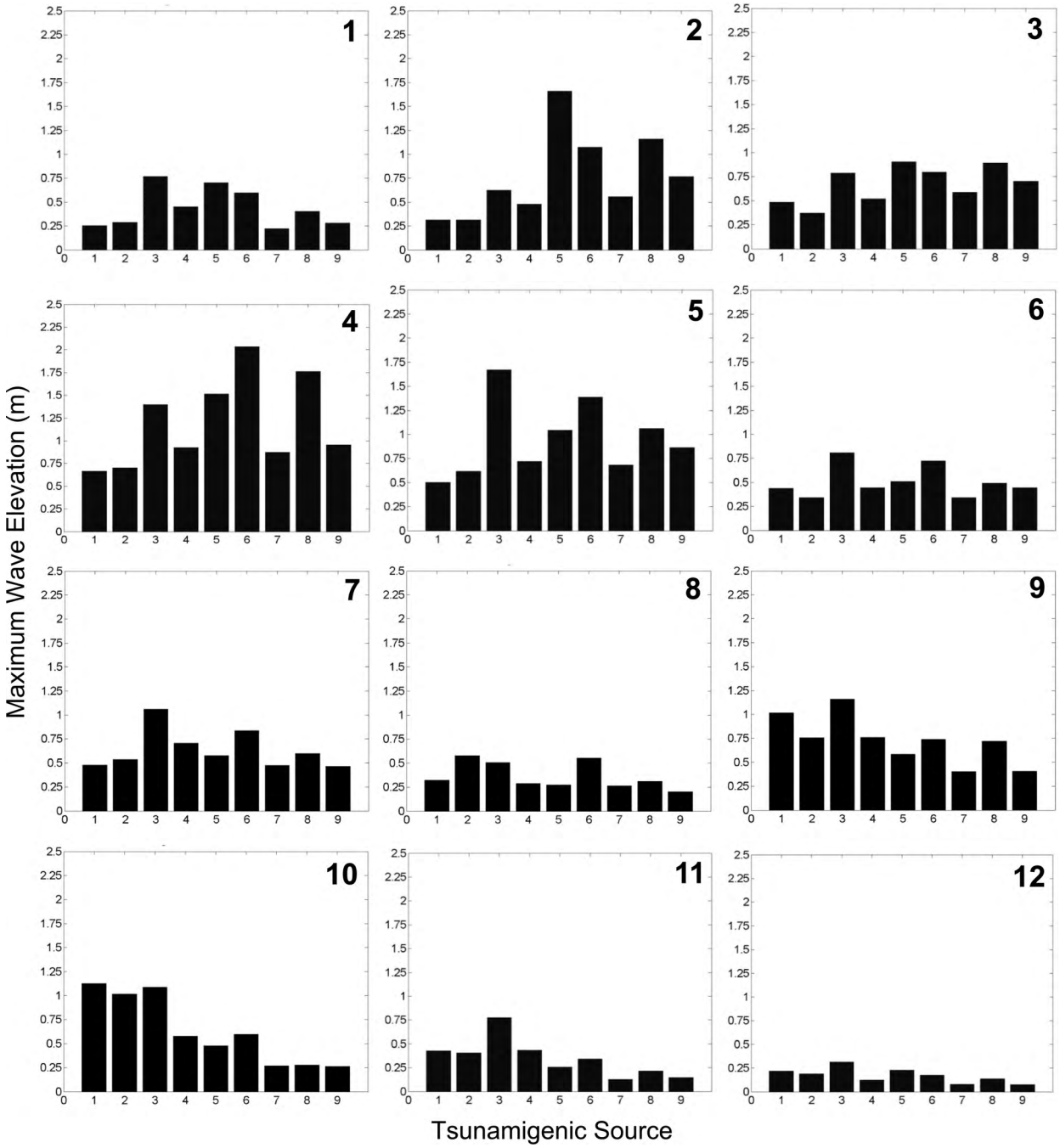

Figure 8. Maximum wave elevation at different points along the eastern coast of Majorca for the considered fault scenarios.

value is larger than those levels observed in the Zemmouri earthquake; as the magnitude of the considered scenario is much greater. The amplification of the tsunami waves around the Balearic coast could be related to the generation and amplification of edge waves around the islands and possible harbour resonance. Edge wave generation could be explained by shelf resonance effects, where the tsunami energy is transferred to the shelf oscillation modes.

Table 5. Tsunami travel time to Majorca (P1 to P12) for tsunamis generated by each potential source (in minutes).

points	S-1 Min.	S-2 Min.	S-3 Min.	S-4 Min.	S-5 Min.	S-6 Min.	S-7 Min.	S-8 Min.	S-9 Min.
P1	71	68	66	64	60	60	62	60	64
P2	80	76	73	71	71	72	76	76	80
P3	51	48	45	43	43	45	50	49	54
P4	48	44	40	40	39	42	47	48	52
P5	38	34	32	31	31	33	39	40	45
P6	38	33	31	31	31	35	41	42	47
P7	47	43	41	43	44	47	54	55	61
P8	58	54	53	55	57	60	68	70	77
P9	54	50	49	52	54	57	64	66	72
P10	52	48	46	48	52	54	62	64	70
P11	62	59	58	62	63	68	74	71	74
P12	64	61	61	64	64	64	66	65	68

S-7 and S-8 sources are good candidates for the 1856 Jijel earthquake. The tsunami generated hit the city of Jijel hard, causing extensive damage to the main buildings. However, its impact on the Balearic Islands was minor. The obtained results show that those tsunamis generated in these specific sources are not very energetic in the Balearic Islands because of their important angular dispersion. In contrast, along the Algerian coast these scenarios show edge waves that create important amplification due to the resonance effect in the Bay of Jijel. In Figure 9, the sea water level time variation at a point located in Jijel Bay is shown. In the same figure the initial surface elevation condition is also depicted. As can be appreciated from the initial condition, the maximum water elevation is 1.5 m, while in Jijel an important amplification of this tsunami wave occurs, reaching sea surface level rises of 3 m.

Conclusions

Based on the historical seismicity and characteristics of the well-known El Asnam 1980 and Boumerdes-Zemmouri 2003 earthquakes, we have defined a characteristic worst probable tsunamigenic seismic source in the northern Algeria area. We have used this source as a typical rupture, adapting it to the structural trends and features that constitute the active tectonic belt of the Tell region in the coastal zone.

Nine potential tsunami sources along the Algerian Coast that threaten the Balearic Islands have been proposed. These sources correspond to known structures recently mapped offshore (S-1, S-2, S-3, S-4, S-5) or to probable offshore continuations of known onshore structures (S-6, S-7, S-8, S-9). Although other seismic sources may exist in the area, and the characteristics of the proposed sources can vary slightly, the sources used in this work can be considered credible worst cases for the tsunami impact on the Balearic Islands.

Numerical models of the nine worst potential events have been tested. It has been shown that catastrophic tsunamis cannot be triggered from these sources in the Balearic Islands. However, wave elevation rises of up to 2 m in water depths of 10 m could generate low level flooding and wave amplifications in bays and harbours.

Numerical simulations have shown important wave energy associated with edge waves, generated by the tsunami interaction with the continental shelf around the Balearic Islands. These shorter wave lengths can generate resonance effects when these

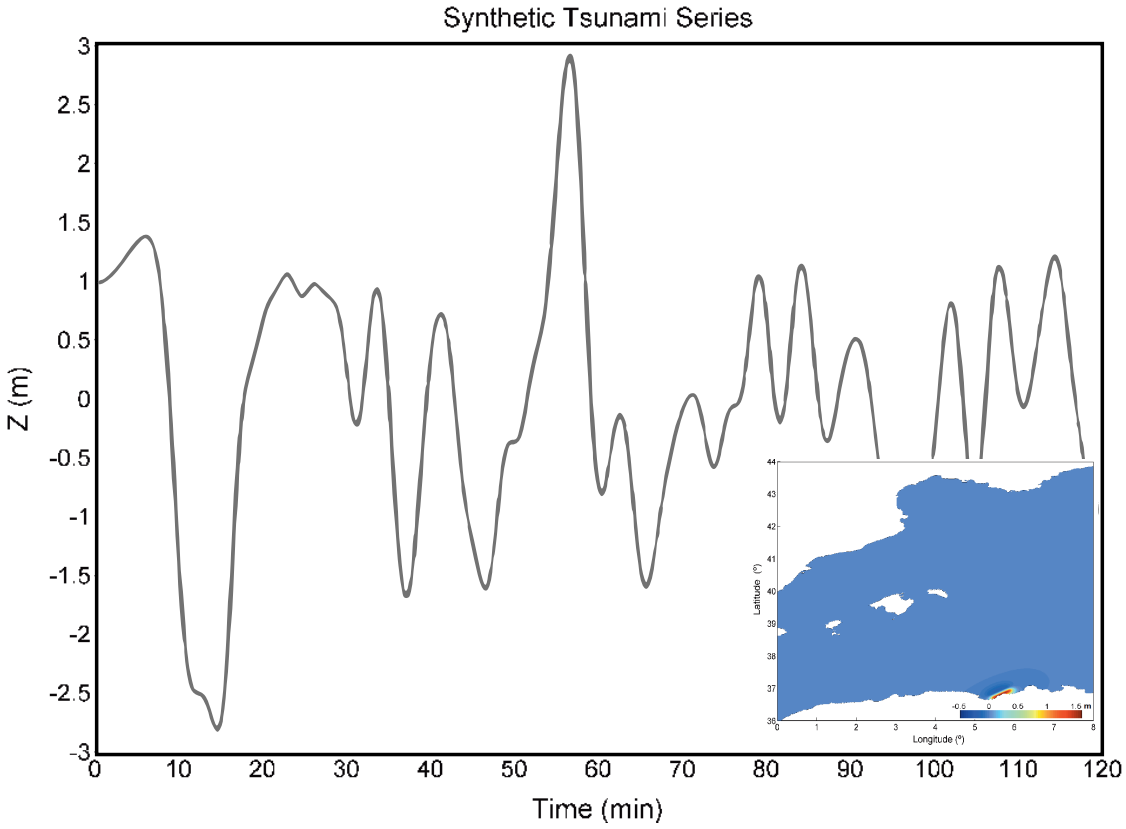

Figure 9. Maximum sea level oscillation at a point inside the bay of Jijel for scenario S-7.

waves arrive in bays and harbours (e.g., Palma, Ibiza, and San Antonio).

Among the proposed sources, the greatest impact on Majorca is associated with the S-3 and S-6 sources, where higher wave elevations are obtained in the southeastern part of the island. However, a tsunami triggered from the source S-8 could generate an important impact on the north and northeast part of the island. The source S-4 has characteristics similar to those of the 2003 Boumerdes-Zemmouri tsunami, although the higher seismic magnitude simulated as the worst case generates greater waves, up to 1 m high.

Sources S-7 and S-8 are good candidates for the 1856 Jijel earthquake and tsunami, especially the former. In the case of Source S-7 the waves are confined mainly to the bays of Béjaïa and Jijel in Algeria, explaining why the damage along the Balearic coasts was slight.

For future tsunamis generated in this region, this preliminary study will help produce rapid estimates of travel time and tsunami elevations along the coasts of Majorca.

Acknowledgements

This work has been developed within the context of the European TRANSFER (Tsunami Risk ANd Strategies For European Region) Project, Sixth Framework Programme 'Assessment and Reduction of Tsunami Risk in Europe'. This is a contribution from the groups: Active Tectonics and Paleoseismicity (UCM-910368) and the Ocean & Coastal Research Group from the Instituto de Hidráulica Ambiental (Universidad de Cantabria). The authors are grateful for the comments and suggestions of two anonymous referees. John A. Winchester edited the English of the final text.

References

Alasset, P.J., Hébert, H., Maouche, S., Calbini, V. & Meghraoui, M. 2006. The tsunami induced by the 2003 Zemmouri earthquake (M_W= 6.9, Algeria): modelling and results. *Geophysical Journal International* **166**, 213–226.

Ambraseys, N.N. 1981. The El Asnam (Algeria) earthquake of 10 October 1980; conclusions drawn from a field study. *Quarterly Journal of Engineering Geology & Hydrogeology* **14**, 143–148.

Aoudia, A., Vaccari, F., Suhadolc, P. & Meghraoui, M. 2000. Seismogenic potential and earthquake hazard assessment in the Tell Atlas of Algeria. *Journal of Seismology* **4**, 79–98.

Bezzeghoud, M., Dimitrov, D., Ruegg, J.C., Lammali, K. 1995. Faulting mechanism of the El Asnam (Algeria) 1954 and 1980 earthquakes from modelling of vertical movements. *Tectonophysics* **249**, 249–266.

Bounif, A., Dorbath, C., Ayadi, A., Meghraoui, M., Beldjoudi, H., Laouami, N., Frogneux, M., Slimani, A., Alasset, P.J., Kharroubi, A., Ousadou, F., Chikh, M., Harbi, A., Larbes, S. & Maouche, S. 2004. The 21 May 2003 Zemmouri (Algeria) earthquake M_W 6.8: relocation and aftershock sequence analysis. *Geophysical Research Letters* **31**, L19606, doi:10.1029/2004GL020586.

Chiarabba, C., Amato, A. & Meghraoui, M. 1997. Tomographic images of the El Asnam fault zone and the evolution of a seismogenic thrust-related fold. J*ournal of Geophysical Research* **102**(B11), 24485–24498.

Delouis, B., Vallée, M., Meghraoui, M., Calais, E., Maouche, S., Lammali, K., Mahsas, A., Briole, P., Benhamouda, F. & Yelles, K. 2004. Slip distribution of the 2003 Boumerdes-Zemmouri earthquake, Algeria, from teleseismic, GPS, and coastal uplift data. *Geophysical Research Letters* **31**, L18607, doi:10.1029/2004GL020687.

DeMets, C., Gordon, R., Argus, D.F. & Stein, S. 1990. Current plate motions. *Geophysical Journal International* **101**, 425–478.

Deschamps, A., Gaudemer, Y. & Cisternas, A. 1982. The El Asnam, Algeria, earthquake of 10 October 1980: Multiple-Source mechanism determined from long-period records. *Bulletin of the Seismological Society of America* **72**, 1111–1128.

Déverchère, J., Yelles, K., Domzig, A., Mercier de Lépinay, B., Bouillin, J.-P., Gaullier, V., Bracène, R., Calais, E., Savoye, B., Kherroubi, A., Le Roy, P., Pauc, H. & Dan, G. 2005. Active thrust faulting offshore Boumerdes, Algeria, and its relations to the 2003 M_W 6.9 earthquake. *Geophysical Research Letters* **32**, L04311, doi:10.1029/2004GL021646.

Domzig, A., Yelles, K., Le Roy, C., Déverchère, J., Bouillin, J.P., Bracène, R., Mercier de Lépinay, B., Le Roy, P., Calais, E., Kherroubi, A., Gaullier, V., Savoye, B. & Pauc, H. 2006. Searching for the Africa-Eurasia Miocene boundary offshore western Algeria (MARADJA'03 cruise). *Comptes Rendus Geoscience* **338**, 80–91.

Galindo-Zaldívar, J., González Lodeiro, F. & Jabaloy, A. 1993. Stress and paleostress in the Betic-Rif Cordilleras (Mioceno to Present). *Tectonophysics* **227**, 105–126.

Harbi, A., Maouche, S. & Benhallou, H. 2003. Re-appraisal of seismicity and seismotectonics in the north-eastern Algeria. Part II: 20th century seismicity and seismotectonics analysis. *Journal of Seismology* **7**, 221–234.

Hébert, H. & Alasset, P.J. 2003. The tsunami triggered by the 21 May 2003 Algiers earthquake. *CSEM / EMSC Newsletter* **20**, 10–12.

Ign (Instituto Geográfico Nacional) 2003. Boletín de sismos próximos 2003, http://www.fomento.es/MFOM/LANG_CASTELLANO/DIRECCIONES_GENERALES/INSTITUTO_GEOGRAFICO/Geofisica/sismologia/informacionsis/bolano03/

Ign (Instituto Geográfico Nacional) 2008. Catálogo de Tsunamis en las costas españolas, http://www.fomento.es/MFOM/LANG_CASTELLANO/DIRECCIONES_GENERALES/INSTITUTO_GEOGRAFICO/Geofisica/sismologia/otras/catsum.htm

King, G. & Vita-Finzi, C. 1981. Active folding in the Algerian earthquake of 10 October 1980. *Nature* **292**, 22–26.

Lorito, S., Tiberti, M. M., Basili, R., Piatanesi, A. & Valensise, G. 2008. Earthquake-generated tsunamis in the Mediterranean Sea: scenarios of potential threats to southern Italy. *Journal of Geophysical Research* **113**, B01301, doi:10.1029/2007JB004943.

Liu, P.L.-F., Cho, Y.-S., Yoon, S.-B. & Seo, S.-N. 1994. Numerical simulations of the 1960 Chilean tsunami propagation and inundation at Hilo, Hawaii, Recent development. *In:* El-Sabh, M.I. (ed), *Tsunami Research.* Kluwer Academic Publishers, 99–115.

Liu, P.L.-F., Cho, Y.-S., Briggs, M.J., Synolakis, C.E. & Kanoğlu, U. 1995. Run-up of solitary waves on a Circular Island. *Journal of Fluid Mechanics* **302**, 259–285.

McClusky, S., Reilinger, R., Mahmoud, S., Ben Sari, D. & Tealeb, A. 2003. GPS constraints on Africa (Nubia) and Arabia plate motions. *Geophysical Journal International* **155**, 126–138.

Meghraoui, M. & Doumaz, F. 1996. Earthquake-induced flooding and paleoseismicity of the El Asnam (Algeria) fault-related fold. *Journal Geophysical Research* **101**, 17617–7644.

Meghraoui, M., Maouche, S., Chemaa, B., Çakir, Z., Aoudia, A., Harbi, A., Alasset, P.-J., Ayadi, A., Bouhadad, Y. & Benhamouda, F. 2004. Coastal uplift and thrust faulting associated with the M_W= 6.8 Zemmouri (Algeria) earthquake of 21 May, 2003. *Geophysical Research Letters* **31**, L19605, doi:10.1029/2004GL020466.

Mickus, K. & Jallouli, C. 1999. Crustal structure beneath the Tell and Atlas Mountains (Algeria and Tunisia) through the analysis of gravity data. *Tectonophysics* **314**, 373–385.

Morel, J.L. & Meghraoui, M. 1996. The Goringe-Alboran-Tell (GALTEL) tectonic zone, a transpression system along the Africa-Eurasia plate boundary. *Geology* **24**, 755–758.

Nábělek, J. 1985. Geometry and mechanism of faulting of the 1980 El Asnam, Algeria, earthquake from inversion of teleseismic body waves and comparison with field observations. *Journal of Geophysical Research* **90**(B14), 12713–12728.

Okada, Y. 1985. Surface deformation due to shear and tensile faults in a half-space. *Bulletin of the Seismological Society of America* **75**, 1135–1154.

Ouyed, M., Meghraoui, M., Cisternas, A., Frechet, J., Gaulon, R., Hatzfeld, D. & Philip, H. 1981. Seismotectonics of the El-Asnam earthquake. *Nature* **292**, 26–31.

Peláez Montilla, J.A., Hamdache, M. & López Casado, C. 2003. Seismic hazard in Northern Algeria using spatially smoothed seismicity. Results for peak ground acceleration. *Tectonophysics* **372**, 105–119.

Philip, H. & Meghraoui, M. 1983. Structural analysis and interpretation of the surface deformations of the El Asnam earthquake of October 10, 1980. *Tectonics* **2**, 17–49.

Ruegg, J.C., Kasser, M., Tarantola, A., Lepine, J.C. & Chouikrat, B. 1982. Deformations associated with the El Asnam earthquake of 10 october 1980: geodetic determination of vertical and horizontal movements. *Bulletin of the Seismological Society of America* **72**, 2227–2244.

Semmane, F., Campillo, M. & Cotton, F. 2005. Fault location and source process of the Boumerdes, Algeria, earthquake inferred from geodetic and strong motion data. *Geophysical Research Letters* **32**, L01305, doi:10.1029/2004GL021268.

Serpelloni, E., Vannucci, G., Pondrelli, S., Argnani, A., Casula, G., Anzidei, M., Baldi, P. & Gasperini, P. 2007. Kinematics of the western Africa-Eurasia plate boundary from focal mechanisms and GPS data. *Geophysical Journal International* **169**, 1180–1200.

Wang, X. & Liu, P.L.-F. 2005. A numerical investigation of Boumerdes-Zemmouri (Algeria) earthquake and tsunami. *Computer Modeling in Engineering & Sciences* **10**, 171–183.

Yagi, Y. 2003. *Preliminary Results of Rupture Process for May 21, 2003 Northern Algeria Earthquake*. http://iisee.kenken.go.jp/staff/yagi/eq/algeria20030521/algeria2003521.html

Yelles, A.K., Déverchère, J., Domzig, A., Bracène, R., Mercier de Lépinay, B., Boudiaf, A., Kherroubi, A., Graindorge, D., Bertrand, G. & Winter, T. 2007. New evidences for offshore recent tectonic activity near Algiers: the Khayr-Al-Din bank, Algeria. *Geophysical Research Abstracts* **9**, 08465.

Yelles, K., Lammali, K., Mahsas, A., Calais, E. & Briole, P. 2004. Coseismic deformation of the May 21st, 2003, M_W= 6.8 Boumerdes earthquake, Algeria, from GPS measurements. *Geophysical Research Letters* **31**, L13610, doi:10.1029/2004GL019884.

Yelles-Chaouche, A.K., Djellit, H. & Hamdache, M. 2003. The Boumerdes -Algiers (Algeria) Earthquake of May 21st, 2003 (M_W= 6.8). *CSEM-EMSC newsletter* **20**, 3–5.

Yielding, G., Ouyed, M., King, G.C.P. & Hatzfeld, D. 1989. Active tectonics of the Algerian Atlas Mountains – evidence from aftershocks of the 1980 EI-Asnam earthquake. *Geophysical Journal International* **99**, 761–788.